INTERNATIONAL JOURNAL OF OPTIMIZATION IN CIVIL ENGINEERING
Int. J. Optim. Civil Eng., 2024; 14(4):629-645

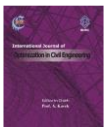

SEISMIC CONFIDENCE LEVELS AND COLLAPSE CAPACITY ASSESSMENT OF STEEL MOMENT RESISTING FRAMES USING NEURAL NETWORKS

A. Hassan Radhi Alhilali, S. Gholizadeh[*, †], and S. Tariverdilo
Department of Civil Engineering, Urmia University, Urmia, Iran

ABSTRACT

This paper employs neural network models to assess the seismic confidence levels at various performance levels, as well as the seismic collapse capacity of steel moment-resisting frame structures. Two types of shallow neural network models including back-propagation (BP) and radial basis (RB) models are utilized to evaluate the seismic responses. Both neural network models consist of a single hidden layer with a different number of neurons. The prediction accuracy of the trained neural network models is compared using two illustrative examples of 6- and 12-story steel moment-resisting frames. The obtained numerical results indicate that the BP model outperforms the RB model in predicting seismic responses.

Keywords: seismic life cycle cost; performance-based design; nonlinear response history analysis; steel moment resisting frame.

Received: 11 November 2024; Accepted: 25 December 2024

1. INTRODUCTION

Seismic design procedures utilize performance-based design [1] to provide adequate seismic resistance for structures at various performance levels. These approaches use nonlinear structural responses to determine the seismic damage levels of structural and nonstructural components. This design process, however, requires significantly more computational effort than other design methods. Structural engineers face the challenge of designing cost-efficient and reliable structures capable of withstanding earthquakes. To address this challenge, performance-based design optimization techniques have been developed, leading to many studies in this field [2-10]. In recent years, metaheuristic algorithms have emerged as a prominent solution. Stochastic natural phenomena inspire these algorithms and their

[*]Corresponding author: Department of Civil Engineering, Urmia University, Urmia, P.O. box 165, Iran
[†]E-mail address: s.gholizadeh@urmia.ac.ir (S. Gholizadeh)

computer implementation is simple [11-13]. However, despite their advantages, the application of these algorithms leads to a high computational burden due to the extensive number of nonlinear structural analyses required. Moreover, the seismic collapse capacity is a critical parameter for structural designers when evaluating the seismic performance of buildings and other structures. An accurate assessment of seismic collapse potential is essential, as the collapse of structures can lead to significant loss of life and substantial economic damages [14]. Therefore, understanding and accurately predicting this parameter is crucial for ensuring the safety and resilience of structures in earthquake-prone areas. Effective evaluation of seismic collapse capacity involves considering various factors, including structural nonlinear modeling, material properties, and the expected seismic demand. The development of reliable and efficient predictive tools is crucial in this context, as it enables accurate predictions while minimizing computational effort. By employing these advanced techniques, structural engineers can design structures that not only adhere to safety standards but also optimize costs and resources effectively.

In recent years, neural networks have gained attention as an alternative solution to alleviate this computational burden. Neural networks can approximate complex functions and capture nonlinear relationships, making them suitable for predicting the seismic performance of structures with reduced computational effort. By integrating neural networks into the design process, structural engineers can achieve accurate predictions while minimizing the need for extensive computational resources. This paper explores the application of neural network models in assessing seismic confidence level (CL) at immediate occupancy (IO) and collapse prevention (CP) performance levels [15] and evaluating the collapse margin ratio (CMR) [16] of steel moment-resisting frame (MFR) structures. Specifically, two types of shallow neural network models, namely back-propagation (BP) and radial basis (RB) are employed to evaluate the seismic responses. Both models consist of a single hidden layer, each with a different number of hidden layer neurons. The accuracy of the trained BP and RBF models is assessed through two illustrative examples including 6-story and 12-story steel MRFs. The numerical results demonstrate the superiority of the BP model over the RB model in predicting the seismic responses of the steel MRFs.

2. SEISMIC CONFIDENCE LEVELS

The performance evaluation procedures outlined in FEMA-350 [15] allow for estimating the confidence level (CL) for structures' ability to meet a specified performance objective. Each performance objective includes a defined structural performance level along with a corresponding hazard level, which must be achieved to ensure that performance. FEMA-350 [15] considers IO and CP performance levels to align with earthquake hazards that have a 50% and 2% probability of exceedance in 50 years, respectively. Predicting building damage for a given level of ground motion is challenging due to numerous uncertain factors affecting building behavior. Analysis procedures are not entirely accurate, and the character of the ground motion itself is uncertain. Therefore, it is inappropriate to imply an absolute performance assessment or the possibility of designing structures that will achieve desired performance objectives. FEMA-350 [15] employs a reliability-based probabilistic approach

to performance evaluation that explicitly accounts for inherent uncertainties. These uncertainties are quantified through a CL. A high CL indicates a strong likelihood that the building will be able to meet the desired seismic performance. The fundamental process of performance evaluation involves developing a mathematical model of the structure and assessing its response to earthquake hazards through nonlinear structural analysis. In this paper, interstory drifts are used as structural response parameters. These parameters reflect the damage sustained by individual structural components and the overall structure [15]. The confidence level for earthquake hazard levels can be computed using the following equation:

$$CL_{IO} = CDF\left(\frac{k\beta_{UT}}{2} - \frac{ln\left(\frac{\gamma\gamma_a D}{\varphi C}\right)}{\beta_{UT}}\right)_{IO} \tag{1}$$

$$CL_{CP} = CDF\left(\frac{k\beta_{UT}}{2} - \frac{ln\left(\frac{\gamma\gamma_a D}{\varphi C}\right)}{\beta_{UT}}\right)_{CP} \tag{2}$$

in which CDF is the normal cumulative distribution function; k is the slope of the hazard curve; β_{UT} is an uncertainty measure; γ is a demand variability factor; γ_a is an analysis uncertainty factor; D is the demand; C is the capacity; and φ is a resistance factor [15].

3. COLLAPSE MARGIN RATIO

FEMA-P695 [16] proposes a methodology based on performing incremental dynamic analysis (IDA) to assess the seismic collapse capacity of structures. This approach requires the implementation of nonlinear response-history analyses using a suite of ground motion records specified by FEMA-P695. The IDA curves are developed by plotting the maximum inter-story drift ratio, $ISD_{\max}$, against the 5% damped spectral acceleration at the structural fundamental period, $S_a(T_1,5\%)$. The collapse margin ratio (CMR) of structures is defined as the ratio of the spectral acceleration for which half of the pre-defined earthquake records cause collapse ($S_a^{50\%}$) to the spectral acceleration of the maximum considered earthquake (MCE) ground motion (S_a^{MCE}) as follows:

$$CMR = \frac{S_a^{50\%}}{S_a^{\mathrm{MCE}}} \tag{3}$$

While the FEMA-P695 methodology is widely used to determine the seismic collapse capacity of structures, it is highly time-consuming due to the need for numerous nonlinear response history analyses.

Shafei et al. [17] proposed a simplified methodology to evaluate CMR spending at a reasonable computational cost. In this simplified methodology, a nonlinear static pushover analysis is performed to derive the pushover curve. Subsequently, an idealized trilinear

pushover curve is generated. As illustrated in Fig. 1, the parameters such as the roof drift ratio in the post-elastic–pre-capping region, ψ_p, roof drift ratio in the post-capping region, ψ_{pc}, and ultimate roof drift ratio, ψ_u can be extracted from the pushover curve. The median collapse capacity, $S_a^{50\%}$, of steel MRFs is evaluated using the following equation [17]:

$$S_a^{50\%} = exp\left(z_0 + z_1\frac{T}{N} + z_2\Gamma_p + z_3\ln\left(\psi_{pc} - \psi_p\right) + z_4\ln\left(\frac{\psi_u - \psi_{pc}}{\psi_{pc} - \psi_p}\right)\right) \quad (4)$$

where N is the number of stories; z_0 to z_4 can be determined using Table 1 (interpolation is necessary for various values of N); and T is the fundamental period.

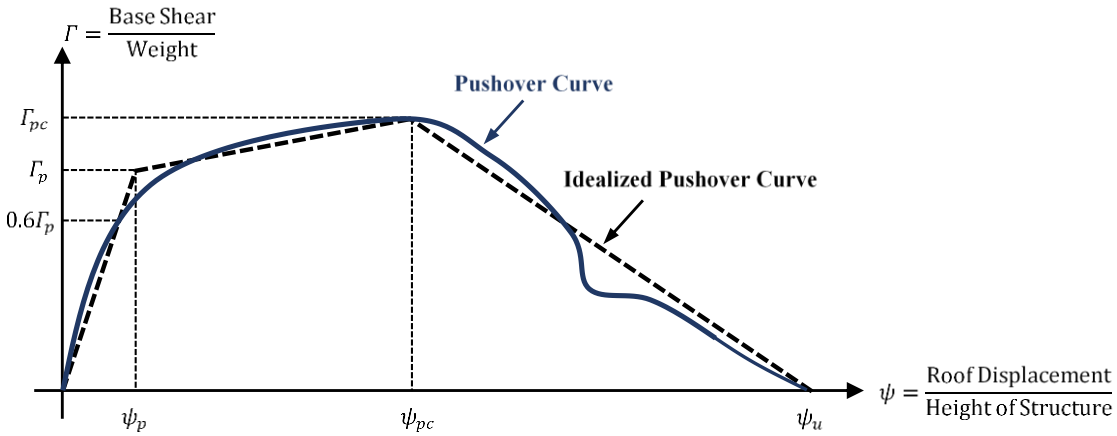

Figure 1. Pushover curves

Table 1: Values of z parameters

Coefficients	N		
	4	8	12
z_0	1.80	2.27	2.49
z_1	–2.30	–4.54	–5.61
z_2	1.76	2.75	3.56
z_3	0.35	0.48	0.13
z_4	0.27	0.16	0.95

4. NEURAL NETWORKS

Neural network (NN) models are efficient tools for addressing complex and time-consuming problems. They are popular due to their ability to learn from external data and past experiences. A significant advantage of a well-trained NN model is its reduced computational burden when producing approximate solutions. Such approximations are valuable in problems where actual response computations are computationally intensive and quick estimations are needed. For these problems, an NN model is trained using data

generated from a series of carefully selected analyses. The data from these analyses are processed to create the necessary input and target pairs, which are then used to train the NN. This paper employs two well-known NN models: back-propagation (BP) [18] and radial basis (RB) [19].

4.1 BP model

The BP model is a multi-layer perceptron trained by a back-propagation [18] technique. Although this model can incorporate multiple hidden layers, this paper focuses on a single hidden layer for simplicity as shown in Fig. 2. The transfer function of the hidden layer neurons is the tangent sigmoid function.

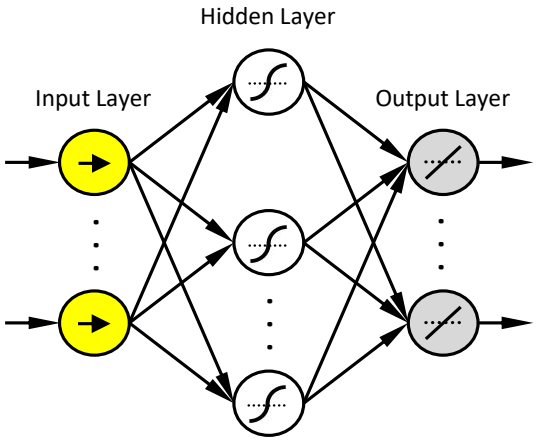

Figure 2. BP neural network model

The training algorithm of the BP model is a gradient descent optimization algorithm that adjusts the weights in the steepest descent direction according to the following equation:

$$W_{t+1} = W_t - \eta \nabla_t \tag{5}$$

where W_t, ∇_t, and η_t are the weight matrix, and the current gradient matrix learning rate, respectively, at iteration t.

The back-propagation technique uses the Levenberg-Marquardt (LM) [18] algorithm to approach second-order training speed without having to compute the Hessian matrix. In the LM algorithm, the updating of the weights is achieved as follows:

$$W_{t+1} = W_t - [J^T J + \alpha I]^{-1} J^T Er \tag{6}$$

where J is the Jacobian matrix, the first derivatives of the network errors to the weights); Er is a vector of network errors; α is a correction factor; and I is the identity matrix.

Regularization is a technique employed to prevent overfitting. It achieves this by modifying the performance function of the model through the addition of a term. This term comprises the mean of the sum of squares of the weights, and is expressed as follows [18]:

$$mse_r = \gamma\left(\frac{1}{m}\sum_{k=1}^{m}(Er_k)^2\right) + \frac{1-\gamma}{nw}\sum_{l=1}^{nw}\left(W_{t,l}\right)^2 \quad (7)$$

where γ and nw are the performance ratio and number of network weights, respectively; and m is the size of Er_k.

4.2 RB model

The RB model is popular due to its fast training, generality, and simplicity. This model is a feedforward NN with a single hidden layer, as illustrated in Fig. 3.

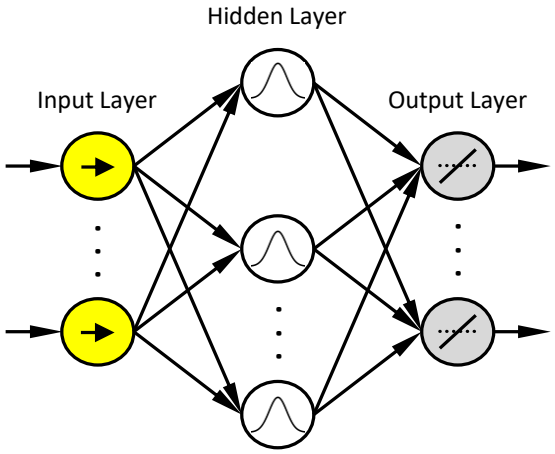

Figure 3. RB neural network model

The hidden layer comprises neurons with Gaussian transfer functions. The outputs of these neurons respond significantly to inputs only within a specific range of values, known as the receptive field. The radius of the receptive field adjusts the sensitivity of the neurons. During training, the receptive field radius is determined so that the neurons can adequately cover the input space. The output layer neurons produce a linear weighted summation of the hidden layer neurons' responses. No actual training is performed to determine the weights of the hidden layer, instead, the transpose of the training input matrix is used as this layer's weight matrix [19].

$$W_1 = \Delta^T \quad (8)$$

where, W_1 and Δ are the input layer weight and the training input matrices, respectively.

A supervised training algorithm is employed to adjust the output layer weights. The output layer weight matrix is determined using the following equation:

$$W_2 = \vartheta^{-1}T \quad (9)$$

where W_2 is the output layer weights; T is target matrix; and ϑ is the hidden layer output.

5. METHODOLOGY

This paper presents two planar steel MRFs with 6 and 12 stories. Figure 4 illustrates their topology and member grouping details. The vectors of design variables of these structures are as follows:

For 6-story MRF $$X = \{C1\ \ C2\ \ \ldots C6\ \ B1\ \ B2\ \ \ldots\ \ B6\}^T \tag{10}$$

For 12-story MRF $$X = \{C1\ \ C2\ \ \ldots C18\ \ B1\ \ B2\ \ \ldots\ \ B12\}^T \tag{11}$$

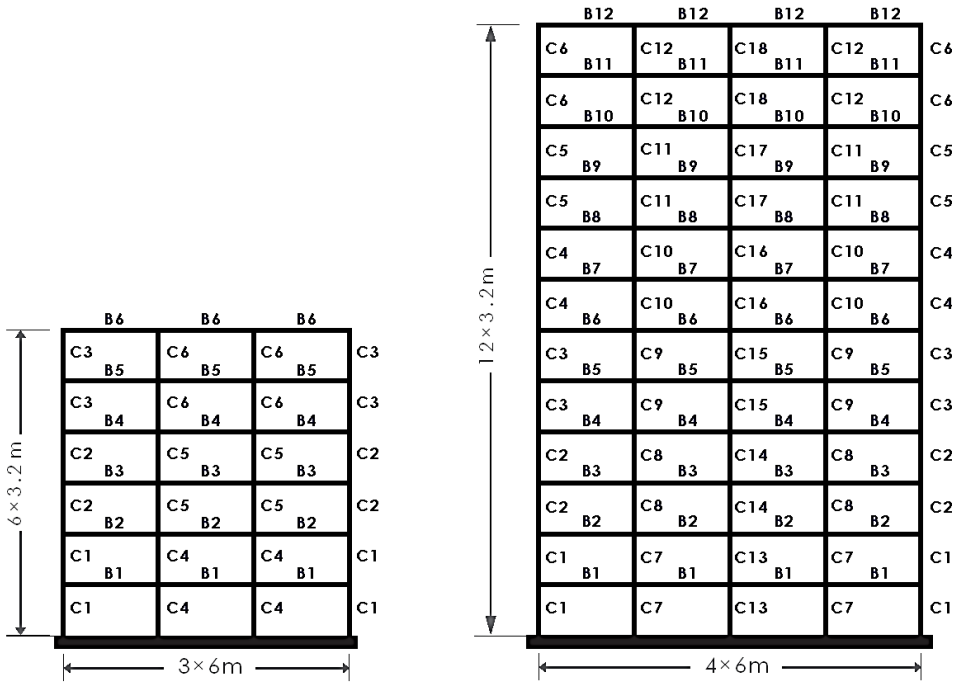

Figure 4. 6 and 12-story steel MRFs

The seismic responses of steel MRFs to be evaluated include confidence level at the IO performance level, CL_{IO}, confidence level at the CP performance level, CL_{CP}, and the collapse margin ratio, CMR. To enhance the efficiency of seismic response evaluation, one NN model is trained to predict CL_{IO} and CL_{CP}. Additionally, another NN is trained to predict CMR. The proposed BP and RB-based NN models are illustrated in Fig. 5.

(a) (b)

Figure 5. (a) BP-based and (b) RB-based NN models

This paper employs a concentrated plasticity approach to simulate the behavior of steel components in MRFs. Using this method, the inelastic behavior of steel components is modeled with multi-linear nonlinear springs, which idealize the moment-chord rotation behavior for beams and columns. The primary advantage of these elements lies in their simplicity and computational efficiency, making them well-suited for simulating the seismic response of steel MRFs [20]. This paper uses the modified Ibarra Medina-Krawinkler concentrated plastic hinge model [21] to model the inelastic nonlinear behavior of beams and columns of steel MRFs. In the frame modeling process, panel zone deformation is neglected, rigid diaphragms are considered, and P-Delta effects are included.

Database generation is the first step in the NN training process. For this paper, all the generated samples for steel MRFs must meet geometric (GEO) strength (STR) and strong column-weak beam (SCWB) constraints.

According to the following GEO constraints, the dimensions of beams and columns at a framing joint, shown in Fig. 6, must be consistent.

$$b_B \leq b_C^{bot} \tag{12}$$

$$b_C^{top} \leq b_C^{bot} \tag{13}$$

$$h_C^{top} \leq h_C^{bot} \tag{14}$$

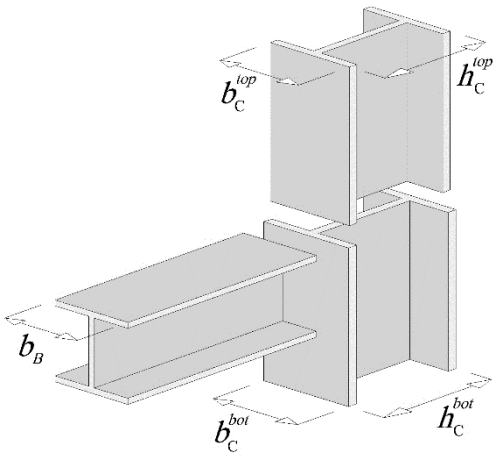

Figure 6. A typical framing joint

According to the STR constraints outlined below, each structural element must satisfy the following requirements for non-seismic load combinations [22]:

$$\text{For} \quad \frac{P_u}{\phi_c P_n} < 0.2 \quad : \quad \frac{P_u}{2\phi_c P_n} + \frac{M_u}{\phi_b M_n} \leq 1.0 \tag{15}$$

$$\text{For} \quad \frac{P_u}{\phi_c P_n} \geq 0.2 \quad : \quad \frac{P_u}{\phi_c P_n} + \frac{8}{9}\frac{M_u}{\phi_b M_n} \leq 1.0 \tag{16}$$

where P_u is the required strength; P_n is the nominal axial strength; ϕ_c and ϕ_b are the resistance factors; M_u and M_n are the required and nominal flexural strengths, respectively.

In accordance with ANSI/AISC 341-16 [23], to delay column hinging, the SCWB constraints must be met in framing joints as follows:

$$M_{Beams} < M_{Columns} \tag{17}$$

in which, M_{Beams} and $M_{Columns}$ represent the sum of the projections of the expected flexural strengths of the beams and columns at framing joints, respectively.

Once a sample structure meets the abovementioned constraints, its seismic responses including CL_{IO}, CL_{CP}, and CMR, are assessed using a nonlinear static pushover analysis based on the displacement coefficient method. Fig. 7 presents a detailed flowchart for the dataset generation process.

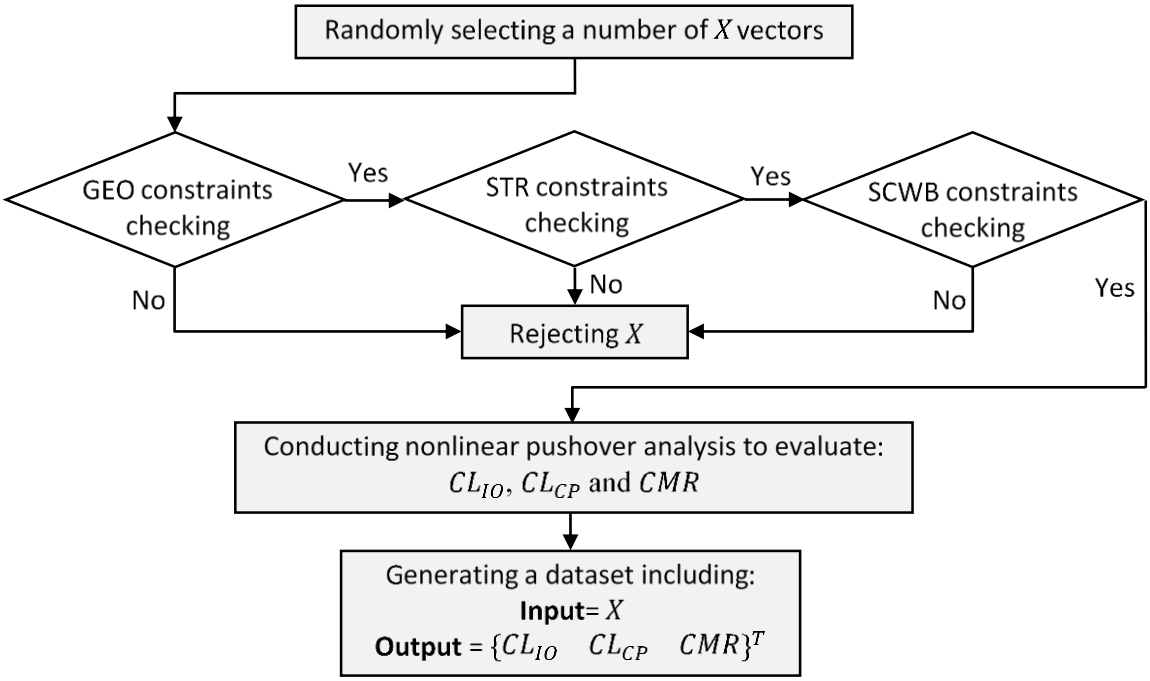

Figure 7. Dataset generation flowchart

The NN model's prediction accuracy evaluation metrics, including Mean Absolute Percentage Error (MAPE), Root Mean Square Error (RSME), and Coefficient of Determination (R-square or R^2) used in this study, are as follows:

Percentage Error $$PE_i = 100\frac{t_i - y_i}{t_i} \tag{18}$$

Mean Absolute Percentage Error $$MAPE = \frac{100}{ns}\sum_{i=1}^{ns}\left|\frac{t_i - y_i}{t_i}\right| \tag{19}$$

Root Mean Square Error $$RMSE = \sqrt{\frac{1}{ns}\sum_{i=1}^{ns}(t_i - y_i)^2} \quad (20)$$

Coefficient of Determination $$R^2 = 1 - \frac{\sum_{i=1}^{ns}(t_i - y_i)^2}{\sum_{i=1}^{ns}(t_i - \bar{t})^2} \quad (21)$$

where ns is the number of data samples; t_i is the ith target response; y_i is the ith predicted response; and $\bar{t}$ is the mean of target responses.

6. NUMERICAL EXAMPLES

The dead load of 2500 kg/m and live load of 1000 kg/m are applied to all beams. The modulus of elasticity and yield stress of materials are E = 210 GPa and F_y = 235 MPa, respectively. The sections of beams and columns are selected from the W-shaped sections listed in Table 2.

Table 2: Available W-shaped sections

Columns				Beams			
No.	Profile	No.	Profile	No.	Profile	No.	Profile
1	W14×48	13	W14×257	1	W12×19	13	W21×50
2	W14×53	14	W14×283	2	W12×22	14	W21×57
3	W14×68	15	W14×311	3	W12×35	15	W24×55
4	W14×74	16	W14×342	4	W12×50	16	W21×68
5	W14×82	17	W14×370	5	W18×35	17	W24×62
6	W14×132	18	W14×398	6	W16×45	18	W24×76
7	W14×145	19	W14×426	7	W18×40	19	W24×84
8	W14×159	20	W14×455	8	W16×50	20	W27×94
9	W14×176	21	W14×500	9	W18×46	21	W27×102
10	W14×193	22	W14×550	10	W16×57	22	W27×114
11	W14×211	23	W14×605	11	W18×50	23	W30×108
12	W14×233	24	W14×665	12	W21×44	24	W30×116

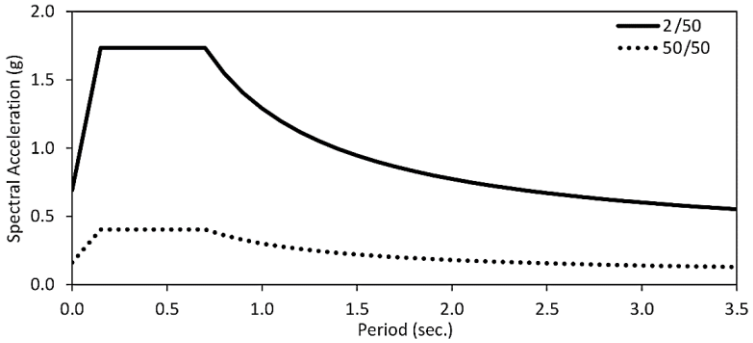

Figure 8. Acceleration response spectra

This paper utilizes acceleration response spectra corresponding to the seismic hazard levels, based on the Iranian seismic design code [24] for soil type III in a region classified as having very high seismicity, as illustrated in Fig. 8.

In addition, details of the modified Ibarra Medina-Krawinkler concentrated plastic hinge model for beams and columns can be found in [8].

6.1 6-story SMF

To train and test the BP and RB-based NN models, a dataset comprising 500 samples is randomly generated. The dataset is divided into training and testing datasets, containing 80% and 20% of the total data, respectively. For the BP-based NN model, 10 hidden layer neurons are considered. The NN models are then trained and tested, with the results reported in Tables 3 and 4, in terms of *MAPE*, *RMSE*, and R^2.

Table 3: Performance evaluation of BP-based NN model for 6-story MRF

Phase	Metric	CL_{IO}	CL_{CP}	*CMR*
Training	*MAPE*	0.8031	0.1116	4.3743
	RMSE	0.0089	0.0019	0.1456
	R^2	0.9967	0.9757	0.8151
Testing	*MAPE*	0.9953	0.0988	4.9870
	RMSE	0.0123	0.0014	0.1692
	R^2	0.9794	0.9370	0.7310

Table 4: Performance evaluation of RB-based NN model for 6-story MRF

Phase	Metric	CL_{IO}	CL_{CP}	*CMR*
Training	*MAPE*	1.8023	0.1488	5.2995
	RMSE	0.0189	0.0019	0.1746
	R^2	0.9852	0.9741	0.7343
Testing	*MAPE*	2.3165	0.2480	6.0146
	RMSE	0.0333	0.0040	0.2034
	R^2	0.8499	0.4671	0.6116

The results indicate that the performance of the BP-based NN model is significantly better than that of the RB-based model. The *MAPE* of the predicted CL_{IO} by the BP-based NN model is 55% lower in the training phase and 57% lower in the testing phase compared to the RB-based NN model. Additionally, the *MAPE* of the predicted CL_{CP} by the BP-based NN model is 25% lower in the training phase and 60% lower in the testing phase than that of the RB-based NN model. Furthermore, for the CMR, the prediction accuracy of the BP-based NN model is 17% better in both the training and testing phases compared to the RB-based model. There are similar results for *RMSE* and R^2.

Fig. 9 displays the regression results for the predicted seismic responses during the training and testing phases of the BP-based NN model. Additionally, Fig. 10 shows the histogram of *PE* for CL_{IO}, CL_{CP}, and CMR highlighting the effective performance of this NN model in estimating the seismic responses of 6-story steel MRF.

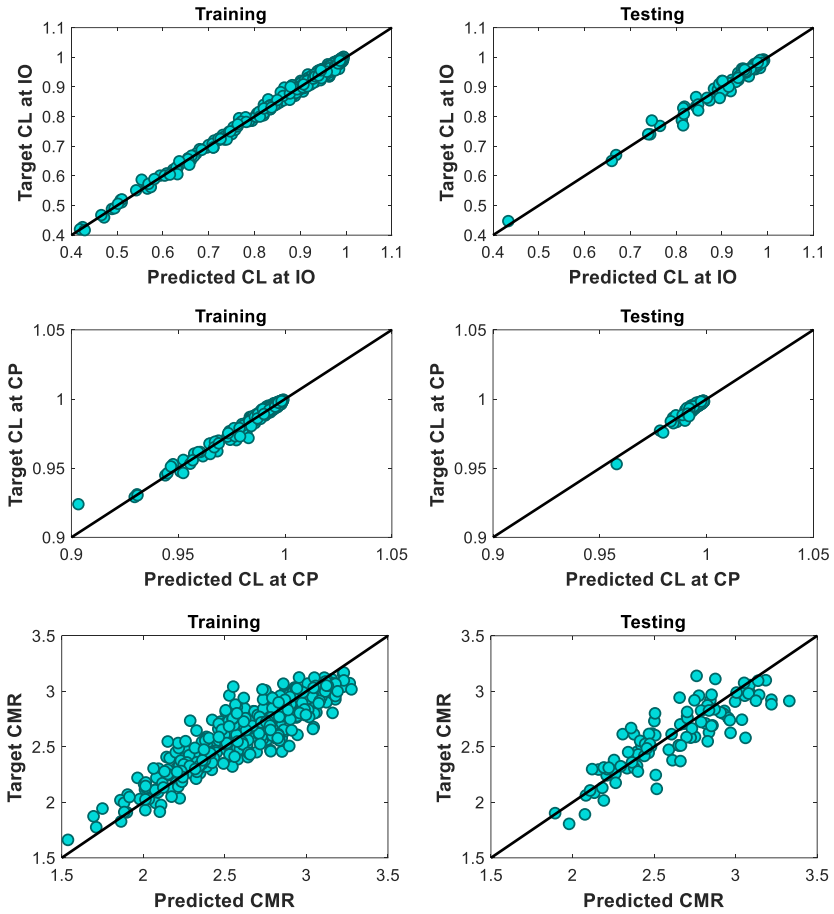

Figure 9. Prediction of CL_{IO}, CL_{CP}, and CMR of 6-story steel MRF

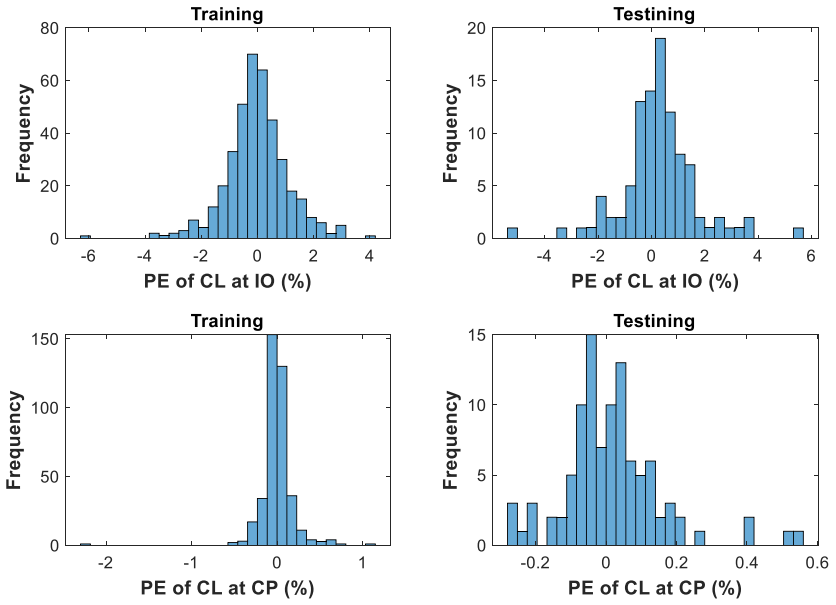

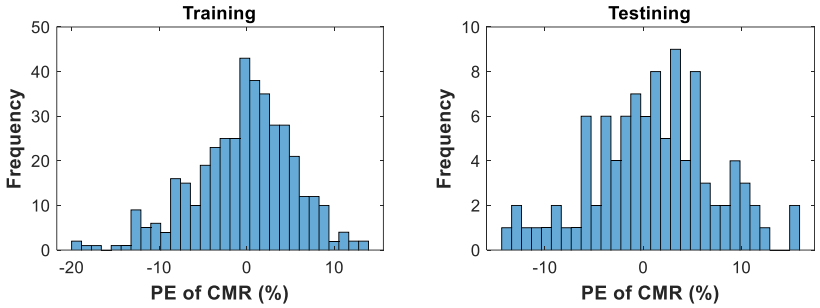

Figure 10. Histogram of PE of CL_{IO}, CL_{CP}, and CMR for 6-story steel MRF

6.2 12-story SMF

In this example, a total of 1000 samples are randomly generated. Out of these, 800 samples are utilized for training, while the remaining 200 samples are allocated for testing. For the BP-based NN model, 10 hidden layer neurons are used. Tables 5 and 6 present the results.

Table 5: Performance evaluation of BP-based NN model for 12-story MRF

Phase	Metric	CL_{IO}	CL_{CP}	CMR
Training	*MAPE*	1.0871	0.3721	2.8948
	RMSE	0.0096	0.0046	0.0633
	R^2	0.9933	0.6711	0.7789
Testing	*MAPE*	1.8648	0.4051	3.8906
	RMSE	0.0163	0.0050	0.0868
	R^2	0.9807	0.6472	0.5877

Table 6: Performance evaluation of RB-based NN model for 12-story MRF

Phase	Metric	CL_{IO}	CL_{CP}	CMR
Training	*MAPE*	3.5432	0.4136	3.3563
	RMSE	0.0295	0.0051	0.0733
	R^2	0.9381	0.6105	0.7039
Testing	*MAPE*	3.8022	0.4654	4.4509
	RMSE	0.0321	0.0055	0.0987
	R^2	0.9260	0.5721	0.4673

The results indicate that the performance of the BP-based NN model is significantly better than that of the RB-based model. The *MAPE* of the predicted CL_{IO} by the BP-based NN model is 69% lower in the training phase and 51% lower in the testing phase compared to the RB-based NN model. Additionally, the *MAPE* of the predicted CL_{CP} by the BP-based NN model is 10% lower in the training phase and 13% lower in the testing phase than that of the RB-based NN model. Furthermore, for the CMR, the prediction accuracy of the BP-based NN model is about 13% better in both the training and testing phases compared to the RB-based model. There are similar results for *RMSE* and R^2.

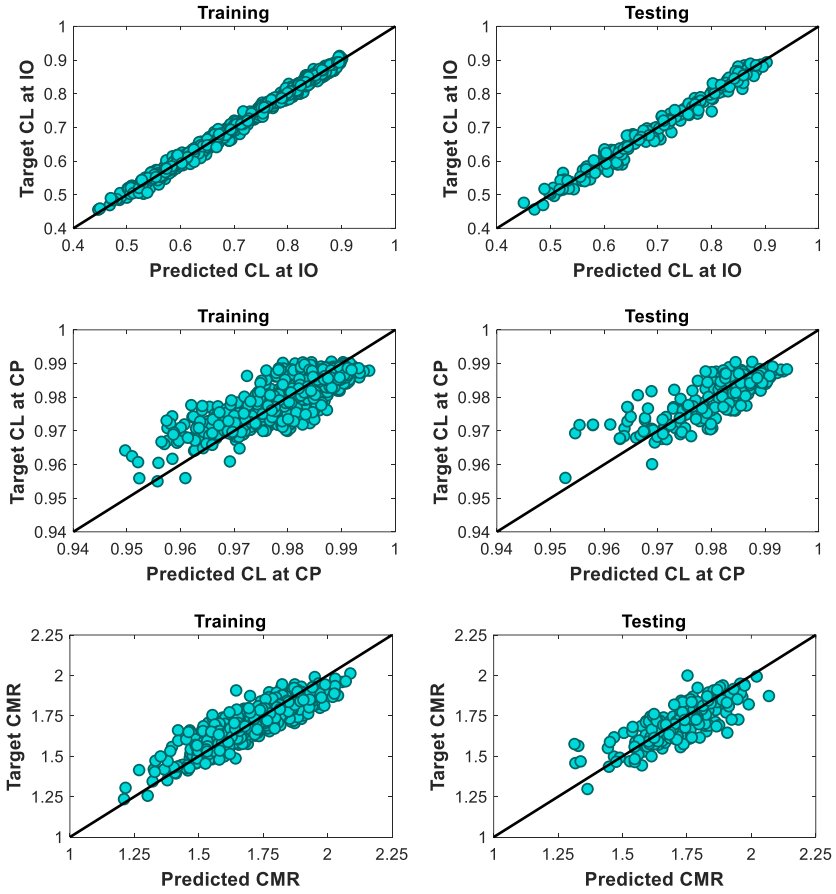

Figure 11. Prediction of CL_{IO}, CL_{CP}, and CMR of 12-story steel MRF

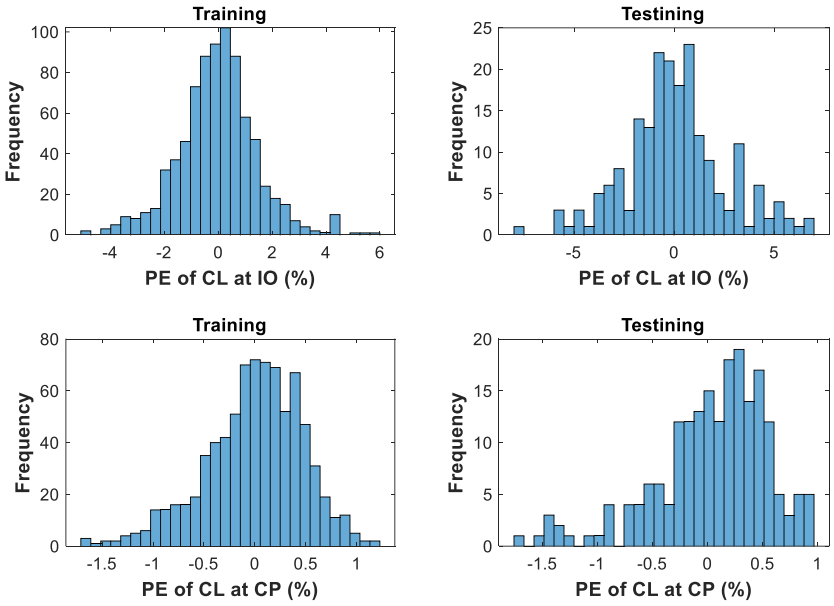

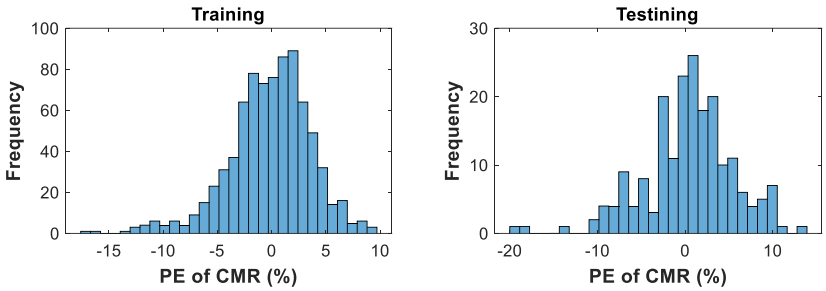

Figure 12. Histogram of PE of CL_{IO}, CL_{CP}, and CMR for 12-story steel MRF

Fig. 11 displays the regression results for the predicted seismic responses during the training and testing phases of the BP-based NN model. Additionally, Fig. 12 shows the histogram of PE for CL_{IO}, CL_{CP}, and CMR highlighting the effective performance of this NN model in estimating the seismic responses of 12-story steel MRF.

7. CONCLUSIONS

The computational cost associated with evaluating the seismic responses of structures through nonlinear pushover analysis is significant. Consequently, this paper focuses on employing neural network (NN) models to estimate the seismic confidence levels at both immediate occupancy and collapse prevention performance levels, in addition to predicting the seismic collapse margin ratio for steel moment-resisting frame structures. Two specific models are utilized for this purpose: a back-propagation (BP) based neural network model and a radial basis (RB) based neural network model. These models aim to enhance the prediction accuracy of the seismic responses of steel frames.

Two numerical examples of 6-story and 12-story steel MRFs are used, with datasets containing 500 and 1000 samples, respectively, being randomly generated for each example. Both BP-based and RB-based NN models are trained and tested using these datasets. The results obtained from this study indicate that the BP-based NN model significantly outperforms the RB-based NN model in estimating seismic confidence levels at both immediate occupancy and collapse prevention performance levels. Additionally, the BP-based model demonstrated superior accuracy in predicting the seismic collapse margin ratio. The BP-based NN model can be effectively incorporated into a performance-based design optimization process to thoroughly explore the design space. It allows for a thorough exploration of the design space while maintaining reasonable computational costs.

REFERENCES

1. FEMA-356, *Prestandard and Commentary for the Seismic Rehabilitation of Buildings*. Federal Emergency Management Agency, Washington DC, 2000.
2. Kaveh A, Laknejadi K, Alinejad B. Performance-based multi-objective optimization of large steel structures. *Acta Mech* 2012; **232**: 355–69.

3. Kaveh A, Zakian P. Performance based optimal seismic design of RC shear walls incorporating soil–structure interaction using CSS algorithm. *Int J Optim Civil Eng* 2012; **2**: 383–405.
4. Ganjavi B, Hajirasouliha I. Optimum performance-based design of concentrically braced steel frames subjected to near-fault ground motion excitations. *Int J Optim Civil Eng* 2019; **9**:177–193.
5. Liang JC, Li LJ, He JN. Performance-based multi-objective optimum design for steel structures with intelligence algorithms. *Int J Optim Civil Eng* 2015; **5**: 79–101.
6. Rahami H, Mohebian P, Mousavi M. Performance-based connection topology optimization of unbraced and X-braced steel frames. *Int J Optim Civil Eng* 2017; **7**:451–468.
7. Gholizadeh S, Hasançebi O. Efficient neural network-aided seismic life-cycle cost optimization of steel moment frames. *Comput Struct* 2024;**301**:107443.
8. Gholizadeh S, Hasançebi O, Eser H, Koçkaya O. Seismic collapse safety based optimization of steel Moment-Resisting frames. *Structures* 2022;**237**:112207.
9. Ghaderi M, Gholizadeh S. Mainshock–aftershock low-cycle fatigue damage evaluation of performance-based optimally designed steel moment frames. *Eng Struct* 2021;**237**:112207.
10. Kaveh A. Applications of artificial neural networks and machine learning in civil engineering, studies in Computational Intelligence 1168, Springer, 2024.
11. Kaveh A, Talatahari S. An enhanced charged system search for configuration optimization using the concept of fields of forces. *Struct Multidiscip Optim*, 2011;**43**:339–351.
12. Kaveh A. Advances in metaheuristic algorithms for optimal design of structures, Springer International Publishing, Switzerland, 3rd edition, 2021.
13. Gholizadeh S, Ebadijalal M. Performance based discrete topology optimization of steel braced frames by a new metaheuristic. *Adv Eng Softw* 2018;**123**:77–92.
14. Zareian F, Krawinkler H. Assessment of probability of collapse and design for collapse safety. *Earthq Eng Struct Dyn* 2007;**36**:1901–14.
15. FEMA-350. Recommended seismic design criteria for new steel moment-frame buildings. Washington (DC): Federal Emergency Management Agency; 2000.
16. FEMA-P695. Quantification of building seismic performance factors. Washington (DC): Federal Emergency Management Agency; 2009.
17. Shafei B, Zareian F, Lignos DG. A simplified method for collapse capacity assessment of moment-resisting frame and shear wall structural systems. *Eng Struct* 2011;**33**:1107–1116.
18. Hagan MT, Demuth HB, Beal MH. Neural network design, PWS Publishing Company, Boston, 1996.
19. Wasserman PD. Advanced methods in neural computing, New York: Prentice Hall Company, Van Nostrand Reinhold, 1993.
20. NIST GCR 17-917-46v2. Guidelines for Nonlinear Structural Analysis for Design of Buildings. Part IIa – Steel Moment Frames. Applied Technology Council, 2017.
21. *OpenSees*. Open System For Earthquake Engineering Simulation. ver 3.3.0 [Computer software]. PEER, Berkeley, CA.

22. ANSI/AISC 360-16. Specification for Structural Steel Buildings. American Institute of Steel Construction. Chicago, Illinois, 2016.
23. ANSI/AISC 341-16. Seismic Provisions for Structural Steel Buildings. American Institute of Steel Construction. Chicago, Illinois, 2016.
24. Standard No. 2800. Iranian Code of Practice for Seismic Resistant Design of Buildings, Building and Housing Research Center, Tehran, 2014.